Pattern Recognition Letters 33 (2012) 543–553

Contents lists available at SciVerse ScienceDirect

Pattern Recognition Letters

journal homepage: www.elsevier.com/locate/patrec

Small object detection in cluttered image using a correlation based active contour model

Alireza Vard *, Kamal Jamshidi, Naser Movahhedinia

Department of Computer Engineering, Faculty of Engineering, University of Isfahan, Isfahan 81746, Iran

ARTICLE INFO

Article history:
Received 16 March 2011
Available online 25 November 2011
Communicated by N. Sladoje

Keywords:
Small object detection
Active contour model
Cluttered image
Correlation

ABSTRACT

This paper presents a novel energy function for active contour models based on autocorrelation function, which is capable of detecting small objects against a cluttered background. In the proposed method, image features are calculated using a combination of short-term autocorrelations (STA) computed from the image pixels to represent region information. The obtained features are exploited to define an energy function for the localized region-based active contour model called normalized accumulated short-term autocorrelation (NASTA). Minimizing this energy function, we can accurately detect small objects in images containing cluttered and textured backgrounds. Moreover, the proposed method provides high robustness against random noise and can precisely locate small objects in noisy backgrounds, difficult to be detected with naked eye. Experimental results indicate remarkable advantages of our approach comparing to existing methods.

1. Introduction

Image segmentation and object detection are the fundamental tasks in image processing and computer vision research, which are utilized in many applications including medicine, remote sensing, industrial inspection and military applications.

In the past decades, numerous approaches have been proposed for image segmentation. Regarding the type of application, each approach could have its relative advantages and disadvantages. Meanwhile, active contour models are one of the well-known segmentation methods, which owing to high accuracy and appropriate flexibility have been widely applied for detecting and segmenting interesting objects in recent years. In this method, an initial contour is defined by the user or constructed automatically in the image. Then, this contour deforms, using an energy function, in order to fit target objects. Energy function is a collection of mathematical rules that are defined according to characteristics of the contour (such as the length of the curve and the area of the inside curve), and interesting image features (such as intensity, color and texture). Then, the energy function is minimized until the contour is conformed to the object boundaries. Active contour models in the context of energy functions and the minimization approach can be broadly divided into two categories: parametric active contour models (Kass et al., 1988; Tauber et al., 2010; Vard et al., 2009; Zhu et al., 2010) and level set active contour models also known as geodesic active contour models (Hua and Liqun, 2008; Savelonas et al., 2008; Shan and Ma, 2010). Parametric active contour is explicitly represented as a set of control points and curve evolution is carried out only on these control points. Therefore, this model is simple and fast, but it has some major drawbacks. Firstly, result of segmentation strictly depends on the initial contour placement and should be defined around the target object. Secondly, this model cannot handle topology changes; on the other hand, contour cannot merge or split and, consequently, it is not possible to find more than one object using this model. Lastly, parametric active contour has self-intersection problem, and the existing solutions for that are computationally complex. To overcome these limitations, level set active contour model has been presented. In this model, contour is implicitly represented as a level set function and the curve evolution is driven by a velocity term that reflects the image features and the contour characteristics. There are two main groups of level set active contour models described in the literature: edge-based active contour models and region-based active contour models. The first group utilizes the image gradient and the edge information in order to guide curve evolution, whereas second group applies the statistical information of image region to lead the motion of the active contour. Region-based active contour models have better performance than edge-based active contour models on noisy images and the images that have weak or blurred object boundaries (Chan and Vese, 2001).

Detecting or extracting small objects in an image is one of the essential challenges in image segmentation, which is used in a variety of applications. For example, extracting small surface defects is an important demand for automatic industrial inspection

* Corresponding author. Tel.: +98 311 7934105; fax: +98 311 7932670.
E-mail addresses: vard@eng.ui.ac.ir, alivard@gmail.com (A. Vard), jamshidi@eng.ui.ac.ir (K. Jamshidi), naserm@eng.ui.ac.ir (N. Movahhedinia).

0167-8655/$ - see front matter © 2011 Elsevier B.V. All rights reserved.
doi:10.1016/j.patrec.2011.11.012

(Abouelela et al., 2005; Ng, 2006). Also, detecting small tumors and nodules in various medical images (e.g. microcalcification detection in mammography) is a valuable tool to assist doctors in the process of disease diagnosis (Bottema and Slavotinek, 2000; Quellec et al., 2011). Other significant applications could be seen in synthetic aperture radar (SAR) images for finding and tracking small targets in military purposes (Huang et al., 2009; Tello et al., 2005). Finding these small objects could be more difficult when the background is complex and cluttered or it has low contrast with interesting objects. In recent years, local energy functions have been introduced for region-based active contour models which make it possible to detect small objects in images with simple background. However, in many real applications, because of image contents, various noise, limitation and external effects of imaging and so on, images have complex and cluttered backgrounds. Unfortunately, existing active contour models cannot correctly find small objects in these images.

In this paper, we introduce a new energy function based on short-term autocorrelation (STA) function for active contours in order to detect small objects in a cluttered and noisy background. In the proposed method, a combination of STA values, called normalized accumulated short-term autocorrelation (NASTA), is calculated from the image pixels to represent region information. The NASTA values are exploited instead of intensity values as a feature to characterize the pixels in our model. This new feature, as will be explained in Section 3, is able to suppress background clutter and enhance dissimilarities between objects and background. Then, these obtained feature values are fused into the energy function of a localized region-based active contour to separate small spots from a cluttered background.

The remainder of this paper is organized as follows: In Section 2, an overview of previous active contour models is presented. The proposed NASTA method is explained in Section 3. The experimental results are presented in Section 4. Finally, the paper is concluded in Section 5.

2. Overview of previous works

Active contour models, which due to shape and movement manner are known as snake models, were firstly introduced by Kass et al. (1988). Snake is a parametric contour, which is steered to interesting features in the image such as lines, edges and corners by minimizing an energy function. In this model, contour is represented as a set of parametric control points and energy function is composed of three parts: internal energy, image energy and external energy. This method was proposed for image segmentation and object tracking, but it had some problems like optimality and convergence for minimizing the energy function. Even though, various works have been performed to improve Kass method, because of intrinsic problems of parametric active contour models that was described in the previous section, these models have less performance than level set active contour models and consequently have less practical applications.

To overcome the limitations of parametric active contour models, Caselles et al. (1993) and Malladi et al. (1995) independently presented geometric active contour models. These models are based on the theory of curve evolution and are numerically implemented via a level set technique. In their methods, contour is implicitly represented as a zero-level set function and the energy function is calculated based on edge information in the image domain. Although these models solve some of the problems of parametric active contour models such as automatic handling of topology changes, they are very sensitive to image noises and weak edges. Furthermore, the results of segmentation highly depend on the location of initial contour.

Chan and Vese (2001) proposed a region-based active contour, well-known as C-V model. This model, which is based on Mumford–Shah model (1989), utilizes statistical information of the image regions instead of applying image gradient in the energy function. The C–V model has several advantages over edge-based active contour: first, it detects object boundaries with weak or blurred edges accurately. Second, the initial contour is not necessary to define around objects and can be located anywhere in the image and finally, this model is less sensitive to image noises. However, the C–V model does not correctly segment images with intensity inhomogeneities.

Segmentation and object detection in images that have intensity inhomogeneities, are discussed in (Vese and Chan, 2002; Tsai et al., 2001). They separately introduced two similar region-based active contour model well-known as piecewise smooth (PS) model. This model can extract objects from a background in the images with intensity inhomogeneity by utilizing a piecewise smooth function. However, the PS model has a complex algorithm with high computational complexity, and, therefore, it is not suitable for practical applications.

Both C-V and PS models exploit the global statistical information in their energy functions, which is not sufficient and precise for detecting small objects against background. In recent years, the localized energy functions have been introduced based on local statistical information of image regions. Local models are more accurate than global models and are suitable for detecting small objects. Examples of localized energies were presented in the work of Lankton and Tannenbaum (2008). In their method, a general framework was proposed for image segmentation with intensity inhomogeneities by re-formulating the global energy functions of region-based active contour and constructing local energy functions. They re-formulated three global energy functions of previous models (which had been introduced by Chan and Vese, 2001; Yezzi et al., 2002; Michailovich et al., 2007) in a local way. Then, they demonstrated advantages of obtained local models comparing to original global models.

Another popular localized region-based active contour is local binary fitting (LBF) model that has been offered by Li et al. (2007, 2008). In this method, two fitting energies are utilized for calculating LBF energy function that approximates the local image intensities on two sides of the contour. These fitting functions are computed for all of the pixels in the image applying a Gaussian kernel. Then, detecting objects is achieved by minimizing the integration of the LBF energy function through the image domain. LBF model, shown in (Li et al., 2008), has better performance than PS model in precise object detection and less computational cost.

Recently, Zhang et al. (2010a) suggested an efficient active contour model based on LBF model. Their method uses a local image fitting (LIF) energy to extract the local statistical information of the image. Indeed LIF energy function determines differences between the fitted image in the LBF model and the original image. In addition, a filtering method with a Gaussian kernel is applied to regularize level set function at each iteration. Consequently, their proposed scheme does not require re-initializing the level set function. The LIF model, shown in (Zhang et al., 2010a), with better computational efficiency, has similar result to the LBF model. This model is suitable for detecting small objects against a simple background. Nevertheless, in the case of cluttered or noisy images, it is unable to extract small objects. In the next section, we introduce a new image feature based on the autocorrelation function and fuse it into the LIF model which makes it possible to find small targets in cluttered images.

Other similar localized energy functions are presented in recent years. We refer the interested reader to (Darolti et al., 2008; He et al., 2010; Wang et al., 2009, 2010; Zhang et al., 2010b).

3. Proposed method

The proposed method is described in two subsections. In Section 3.1, we explain a new feature extraction method based on autocorrelation function. Then, in Section 3.2, we combine this

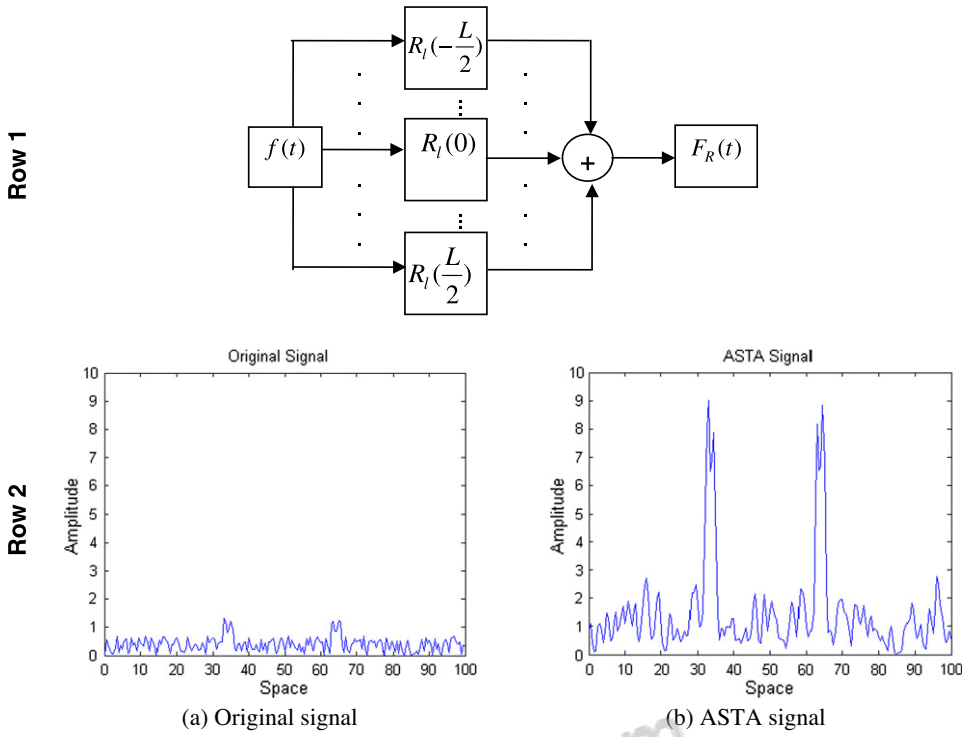

(a) Original signal (b) ASTA signal

Fig. 1. Row 1: ASTA calculation for a small window around index t of the signal f. Row 2: example of applying ASTA function for detecting peaks in a cluttered signal.

new feature into the energy function of a localized region-based active contour and propose a novel energy function for detecting small objects encumbered by dense texture, heavy clutter or noise.

3.1. Feature extraction method

In this subsection, at first we describe our feature extraction method based on autocorrelation function for 1-D signals. Next, we extend it to 2-D signals and introduce a new feature image.

The autocorrelation of a stationary discrete process $f(m)$ at lag k is defined as (Papoulis and Unnikrishna, 2002):

$$R(k) = E(f(m+k)f^*(m)) \tag{1}$$

E is the expected value operator and f^* is the complex conjugate of f, where for a real function, $f = f^*$. This function for an ergodic real signal is defined as:

$$R(k) = \sum_m f(m)f(m+k) \tag{2}$$

This function measures the similarity between signal $f(m)$ and a shifted version of itself. A high value of autocorrelation specifies that the original and shifted signals are highly similar. Conversely,

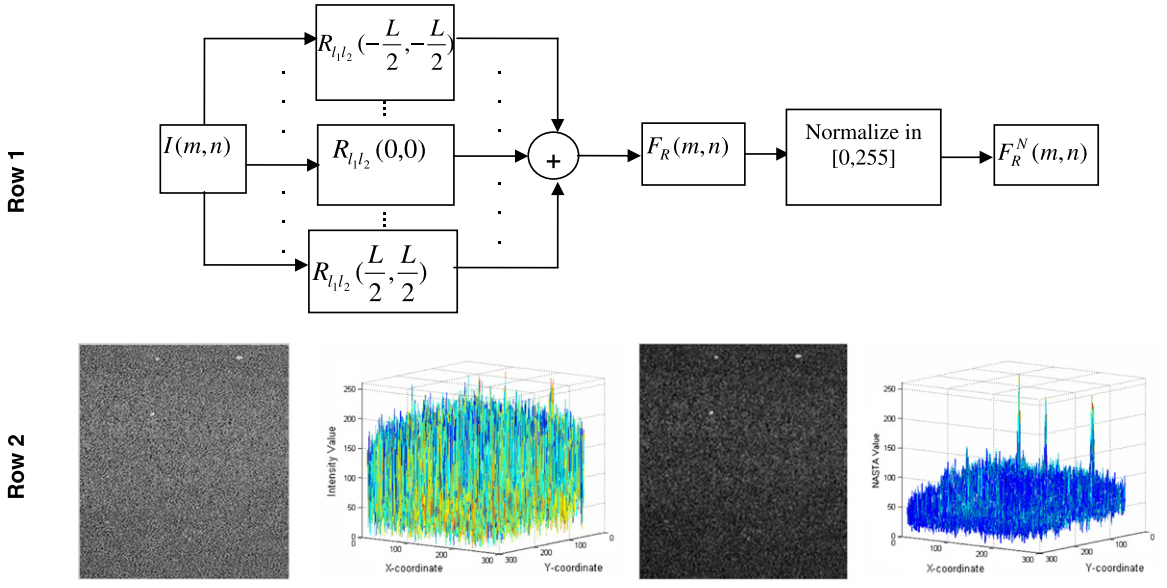

(a) Original image (b) Surface plot of intensity values of original image (c) NASTA feature image (d) Surface plot of NASTA values

Fig. 2. Row 1: NASTA calculation for a small window around pixel (m,n) of an image I. Row 2: example of applying new NASTA image feature for detecting small objects in a cluttered background.

a low autocorrelation value indicates that the signal and its shifted version are weakly related. Autocorrelation function can provide valuable information about periodic events, so it can be utilized to detect the period of repetitive incidents. For accurate localization such as target position detection, the short-term (time) autocorrelation (STA) function may be applied in which the signal is windowed to overlap or non-overlap small sections. STA for a real signal is defined as (Rabiner and Schafer, 1978):

$$R_l(k) = \sum_m f(m)w(l-m)f(m+k)w(l-k-m) \tag{3}$$

where $w(l)$ is a small window of length L. In our proposed method, STA is calculated from $R_l(-L/2)$ to $R_l(L/2)$ in a small window $w(l)$ around every index t of the signal $f(t)$. Next, we take the sum of the obtained STA values and put the yield in the position t as shown in Fig. 1(row 1). Then, a new function (signal) F_R is generated with the same length as the original signal f and the summation of STA in a small window around the index as the value. We call this new function as accumulated short-term autocorrelation (ASTA) and show that it is an appropriate function to find targets in a cluttered signal.

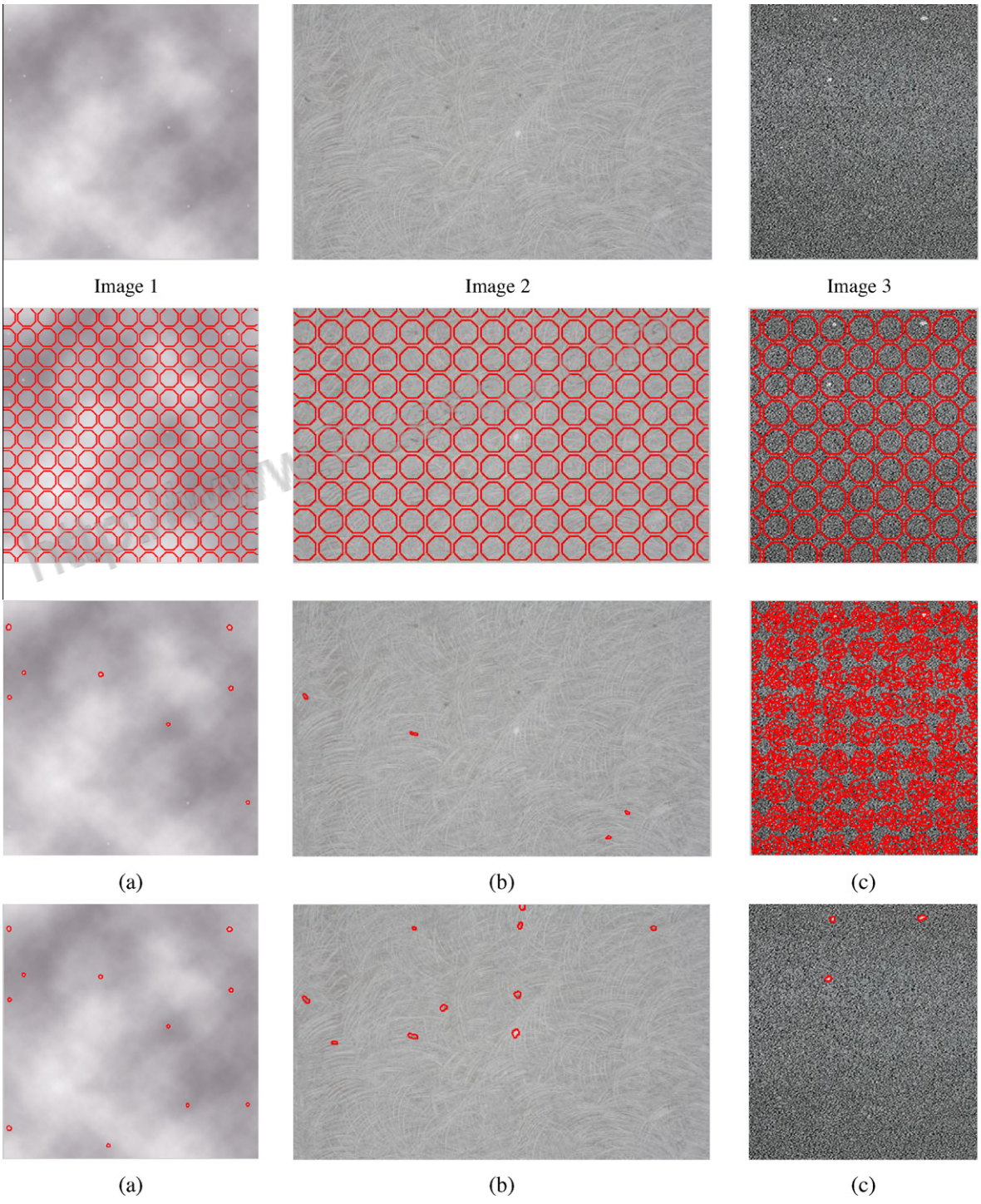

Fig. 3. Results of detecting small targets against homogeneously textured backgrounds for two active contour models. Row 1: original images. Row 2: initial contours. Row 3: results of the LIF model. Row 4: results of the NASTA model.

To illustrate the capability of ASTA for detecting peaks, we consider the 1-D signal shown in Fig. 1(row 2(a)), which indicates two peaks not clearly distinguishable from the remaining parts of the signal. Calculating ASTA function for this signal, Fig. 1(row 2(b)) is obtained in which the two peaks are obviously visible from the other parts of the signal.

Using 2-D short-term autocorrelation function (2D-STA), ASTA can be extended to 2-D image signals. 2D-STA for the image I is defined at horizontal lag k_1 and vertical lag k_2 as:

$$R_{l_1 l_2}(k_1,k_2)=\sum_m\sum_n I(m,n)w(l_1-m,l_2-n)\times I(m+k_1,n+k_2)w(l_1-k_1-m,l_2-k_2-n) \quad (4)$$

where $w(l_1, l_2)$ is a 2-D small sliding window with size of $L \times L$. In our proposed method, this function is computed for the central part of horizontal and vertical lags with the same window size. First, 2D-STA is calculated from $R_{l_1 l_2}(-L/2,-L/2)$ to $R_{l_1 l_2}(L/2,L/2)$ for every pixel (m,n) of image I in a small window around the pixel. Next, the sum of these 2D-STA values is normalized in the range of 0 to 255 and placed in the location index (m,n) (Fig. 2(row 1)). Completing this procedure, a new feature image F_R^N is generated which has the same size as the original image I and the normalized summation of 2D-STAs in a small window around each pixel as the feature value. We called this new feature image as normalized accumulated short-term autocorrelation (NASTA) that is very powerful for extracting targets in a cluttered image.

The proposed method, shown in the first row of Fig. 2, has been chosen for the following reasons. When the image signal is composed of textures and clutters, the pixel value (the STA value in our work) does not provide applicable and significant information. Indeed, the analysis of such an image needs the region information rather than the pixel information. Moreover, the value of a pixel is very sensitive to the noise, which consequently reduces the robustness of segmentation algorithm. Accordingly, we comprehend from our experiments that replacing the current pixel value by the normalized sum of STA values in a window, can be a powerful feature descriptor for textures and clutters. Also, it is more robust against random noise.

The strength of NASTA in object detection is investigated by the example image, shown in Fig. 2(row 2(a)) where some small objects are buried in the cluttered background. Fig. 2(row 2(b)) presents the surface plot of intensity values of this image. As it could be seen in Fig. 2(row 2(b)), the surface plot of intensity values of the objects and the background are not easily distinguishable. Therefore, object extraction is very difficult. In contrary, as it is visible in Fig. 2(row 2(c)), the obtained image by NASTA is properly able to suppress the background clutter and amplify the difference between the interesting objects and the background. Noticing the surface plot of NASTA values in the image domain, which is shown in Fig. 2(row 2(d)), the contrast between objects and background could be obviously recognized as three peaks in the image. This example confirms that the NASTA values are better than the intensity values for detecting the small objects in a cluttered background.

3.2. NASTA-based active contour model

In the proposed method, the NASTA values are utilized as the statistical information of the pixels in the image. These values are adapted into a local region-based active contour to introduce a new NASTA-based active contour model. In this work, we select a local region-based active contour owing to local statistical information being less sensitive to heterogeneity in the image rather than global information. Besides, using local active contour is more efficient for detecting small objects in a cluttered background. We first define a local fitted NASTA (LFN) image, inspired by the LIF model (Zhang et al., 2010a), as:

$$I^{\mathrm{LFN}}=M_1H_\varepsilon(\phi)+M_2(1-H_\varepsilon(\phi)) \quad (5)$$

where M_1 and M_2 are defined as:

$$\begin{cases} M_1=\mathrm{mean}\left(F_R^N\in(\{\boldsymbol{x}\in\Omega|\phi(\boldsymbol{x})<0\}\cap G_\sigma(\boldsymbol{x}))\right)\\ M_2=\mathrm{mean}\left(F_R^N\in(\{\boldsymbol{x}\in\Omega|\phi(\boldsymbol{x})>0\}\cap G_\sigma(\boldsymbol{x}))\right)\end{cases} \quad (6)$$

where F_R^N is the NASTA image and G_σ is a local Gaussian window with standard deviation σ. In Eq. (6), size of the window is determined as $4\lfloor\sigma\rfloor+1\times4\lfloor\sigma\rfloor+1$. Changing the standard deviation σ, the local window size can be varied from a small neighbourhood to the whole image (Zhang et al., 2010a). By increasing the window size, the significance of the global properties is magnified against the local properties, thus, the suitable size of the window is determined according to the application.

The energy function of the NASTA model based on the difference between the NASTA image and the LFN image is formulated as:

$$\begin{aligned}E^{\mathrm{NASTA}}(\phi)&=\frac{1}{2}\int_\Omega\left|F_R^N(\boldsymbol{x})-I^{\mathrm{LFN}}(\boldsymbol{x})\right|^2d\boldsymbol{x}\\&=\frac{1}{2}\int_\Omega\left|F_R^N(\boldsymbol{x})-M_1(\boldsymbol{x})H_\varepsilon(\phi(\boldsymbol{x}))-M_2(\boldsymbol{x})(1-H_\varepsilon(\phi(\boldsymbol{x})))\right|^2d\boldsymbol{x}\\&\boldsymbol{x}\in,\Omega\end{aligned} \quad (7)$$

where $\Omega\subset\Re^2$ is the image domain.

In order to maintain stable evaluation of level set function, we exploit the following distance regularization term (Li et al., 2010):

$$R_p(\phi)=\int_\Omega p(|\nabla\phi|)d\boldsymbol{x},\quad \boldsymbol{x}\in\Omega \quad (8)$$

where $p:[0,\infty)\to\Re$ is a potential function and according to (Li et al., 2010), it is defined as:

$$p(|\nabla\phi|)=p_1(|\nabla\phi|)=\frac{1}{2}(|\nabla\phi|-1)^2 \quad (9)$$

or

$$p(|\nabla\phi|)=p_2(|\nabla\phi|)=\begin{cases}\frac{1}{(2\pi)^2}(1-\cos(2\pi|\nabla\phi|)), & |\nabla\phi|\leqslant1\\ \frac{1}{2}(|\nabla\phi|-1)^2, & |\nabla\phi|\geqslant1\end{cases} \quad (10)$$

In this paper we use $p_2(10)$ for the potential function. Consequently, the total energy function of proposed active contour model is defined as follows:

$$\begin{aligned}E(\phi)&=\lambda E^{\mathrm{NASTA}}(\phi)+\mu R_p(\phi)\\&=\frac{\lambda}{2}\int_\Omega|F_R^N(\boldsymbol{x})-M_1(\boldsymbol{x})H_\varepsilon(\phi(\boldsymbol{x}))-M_2(\boldsymbol{x})(1-H_\varepsilon(\phi(\boldsymbol{x})))|^2d\boldsymbol{x}\\&\quad+\mu\int_\Omega p(|\nabla\phi|)d\boldsymbol{x},\end{aligned} \quad (11)$$

where λ and μ are two positive constant. Applying the steepest descent method (Aubert and Kornprobst, 2006), the energy function

Table 1
Comparative results of detecting small targets for two methods.

Image	Method	Number of all targets	NTD	NFD	NMD
Image 1	LIF model	11	8	0	3
	NASTA model		11	0	0
Image 2	LIF model	9	2	2	7
	NASTA model		9	1	0
Image 3	LIF model	3	0	∞	3
	NASTA model		3	0	0

$E(\phi)$ with respect to ϕ is minimized by solving the gradient flow equation as follows:

$$\phi^{n+1} = \phi^n + \Delta t\{\lambda[(F_R^N - M_1 H_\varepsilon(\phi) - M_2(1 - H_\varepsilon(\phi)))(M_1 - M_2)\delta_\varepsilon(\phi)] + \mu \mathrm{div}(d_p(|\nabla\phi|)\nabla\phi)\} \quad (12)$$

where Δt is the time step, ∇ and $\mathrm{div}(\cdot)$ are gradient and divergence operators respectively, and the function d_p is defined as:

$$d_p(|\nabla\phi|) = \frac{p'(|\nabla\phi|)}{|\nabla\phi|}$$

In the above equations H_ε and δ_ε are smoothed description of the Heaviside step function and the Dirac delta function respectively that are approximated as:

$$H_\varepsilon(z) = \frac{1}{2}\left[1 + \frac{2}{\pi}\arctan\left(\frac{z}{\varepsilon}\right)\right], \quad \delta_\varepsilon(z) = \frac{1}{\pi}\cdot\frac{\varepsilon}{z^2 + \varepsilon^2} \quad z \in \Re \quad (13)$$

For smoothing and maintaining the regularity of contour, we also perform, in the same way proposed in (Zhang et al., 2010a), a filtering operation on level set function at each iteration as follows:

$$\phi = \phi * G_\rho \quad (14)$$

where ρ is a standard deviation of the Gaussian filter G_ρ. In order to improve smoothing influence, the ρ parameter should be selected larger than the square root of the time-step Δt.

The main stages of the proposed scheme for detecting small objects in cluttered images can be summarized as:

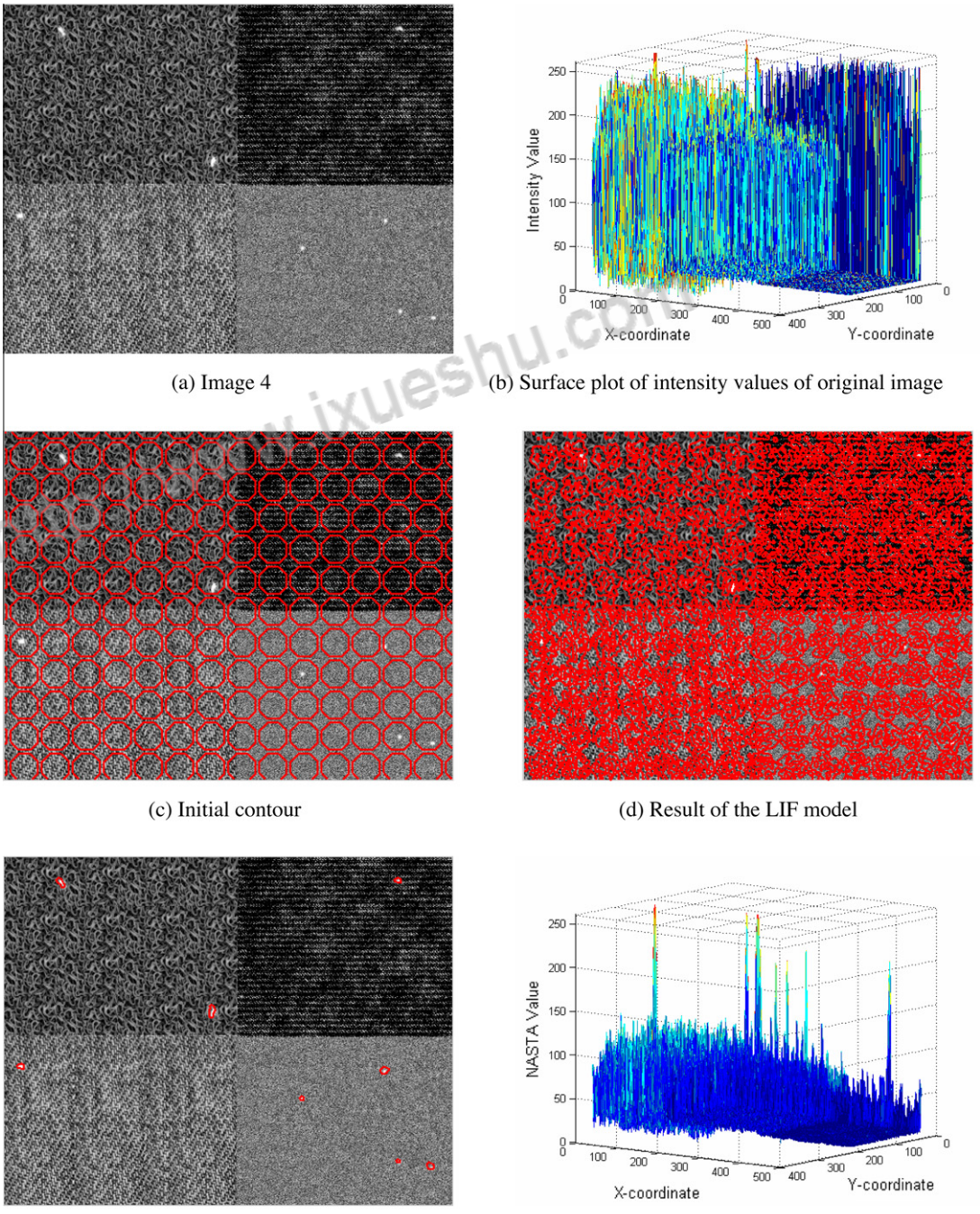

(a) Image 4

(b) Surface plot of intensity values of original image

(c) Initial contour

(d) Result of the LIF model

(e) Result of the NASTA model

(f) Surface plot of NASTA values

Fig. 4. Small object detection against a heterogeneously textured background.

Stage 1: Compute NASTA values for the input image according to the method described in Section 3.1 (Fig. 2(row 1)). To calculate the NASTA values, we set the size of the small window $w(l_1, l_2)$ to 3×3 or 5×5 pixels.

Stage 2: Determine proper values for the parameters of the active contour model. We applied the same parameter as $\varepsilon = 1$ for $\delta_\varepsilon(\phi)$ and $H_\varepsilon(\phi)$, $\lambda = 1$, $\mu = 1$, time step Δt equal to 0.04 and $\sigma \in [0.45, 0.9]$ for the local Gaussian window G_σ in all experiments.

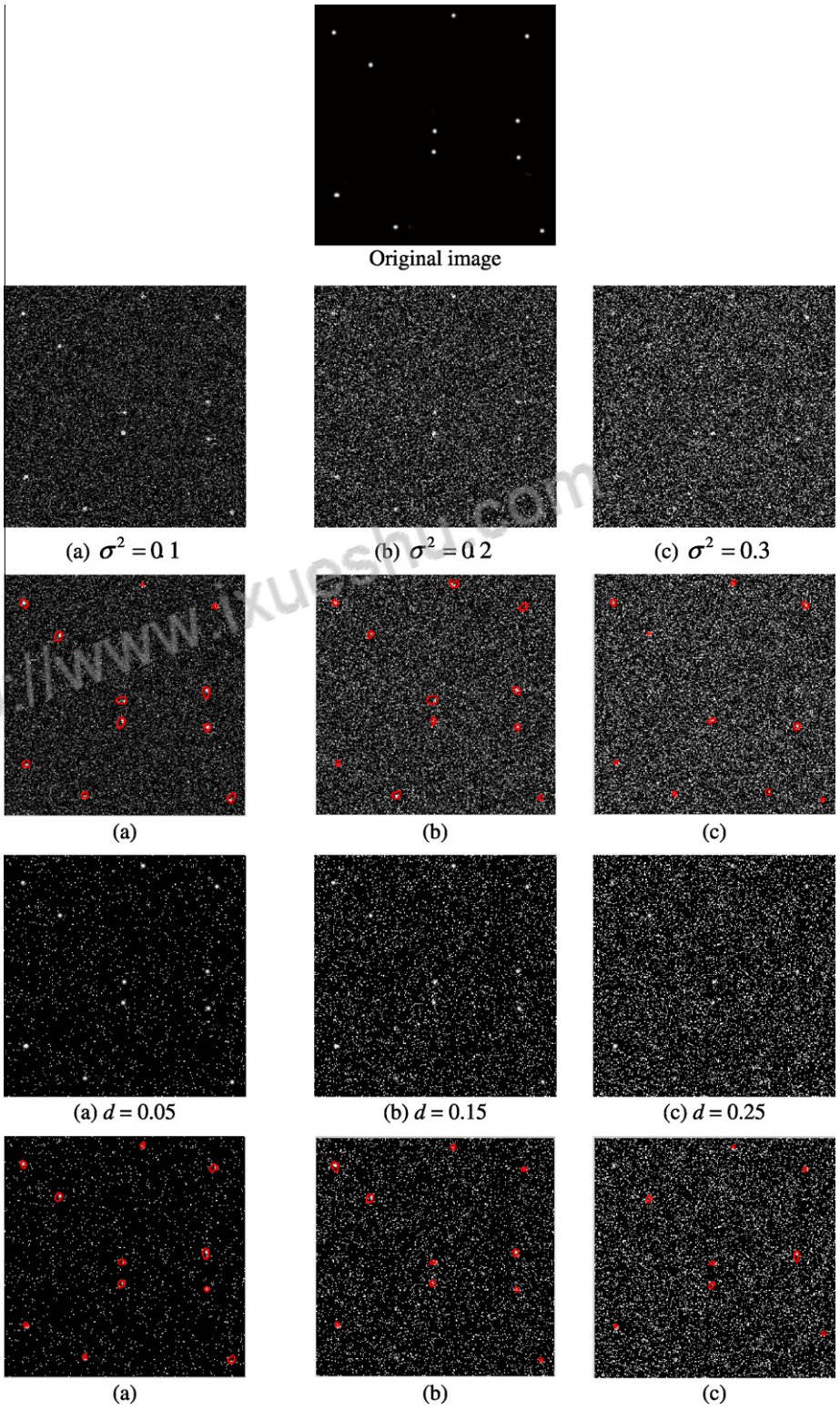

Fig. 5. Considering effect of noise on the proposed method. Row 1: original synthetic image. Row 2: noisy images obtained by adding Gaussian white noise to the original image. Row 3: results of the proposed method corresponding to the noisy images of row 2. Row 4: noisy images obtained by adding Salt & Pepper noise to the original image. Row 5: results of the proposed method corresponding to the noisy images of row 4.

Stage 3: Initialize level set function as follows ($n = 0$):

$$\phi^0(\boldsymbol{x}) = \begin{cases} -1 & \boldsymbol{x} \in \Omega_0 - \partial\Omega_0 \\ 0 & \boldsymbol{x} \in \partial\Omega_0 \\ +1 & \boldsymbol{x} \in \Omega - \Omega_0 \end{cases}$$

where Ω_0 is the subset of the image domain Ω and $\partial\Omega_0$ is the boundary of Ω_0.

Stage 4: Solve the Eq. (12) to obtain ϕ^{n+1}.

Stage 5: Smooth and regularize the contour by the Gaussian filter (Eq. (14)). We selected $\rho = 1$ for the standard deviation of this filter and 5×5 for its window size.

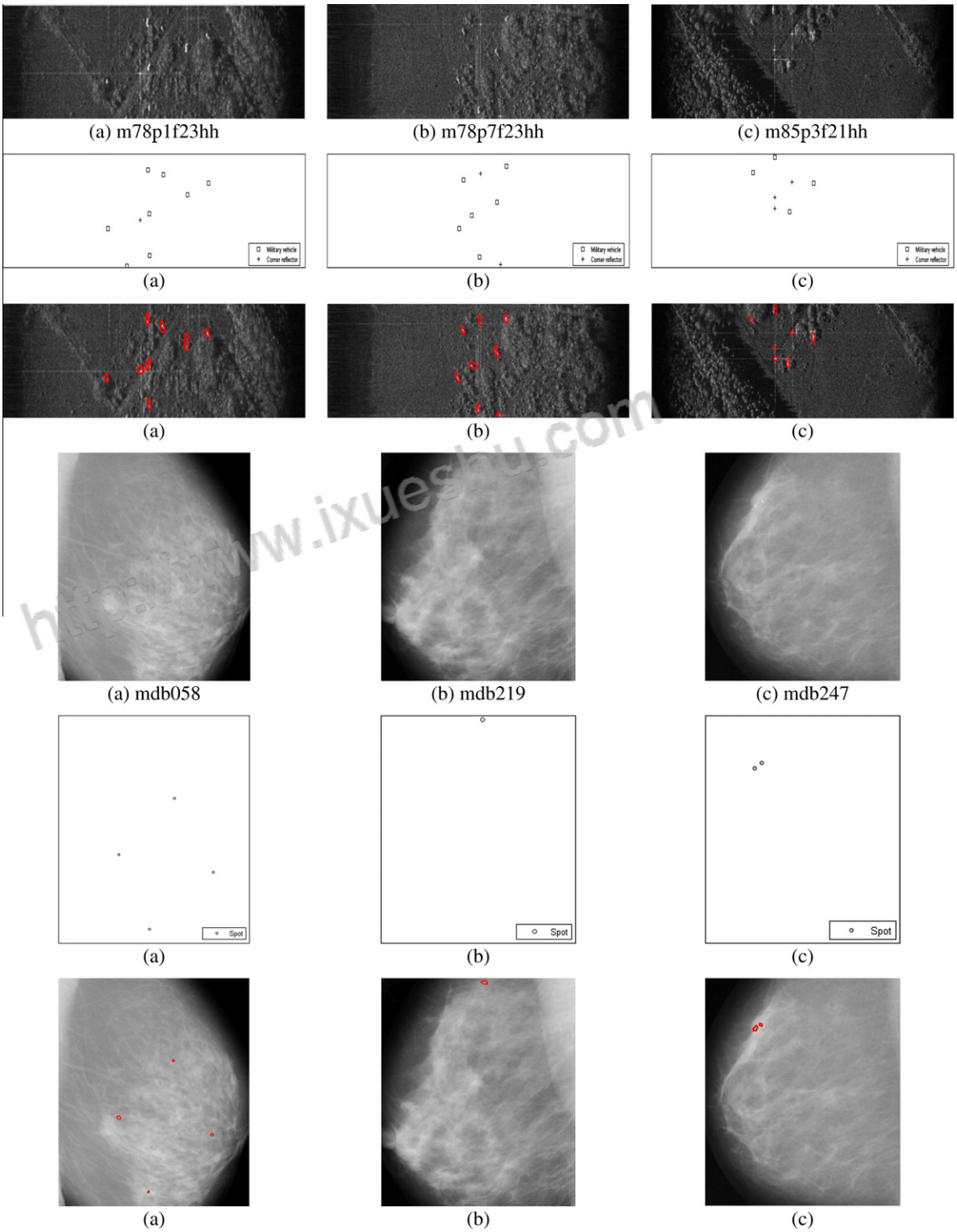

Fig. 6. Application of the proposed method on real images. Row 1: original SAR images. Row 2: ground truth images corresponding to the SAR images of row 1. Row 3: results of the proposed method corresponding to the SAR images of row 1. Row 4: original mammography images. Row 5: ground truth images corresponding to the mammography images of row 4. Row 6: results of the proposed method corresponding to the mammography images of row 4.

Table 2
Target detection results of proposed method in the presence of noise.

(a) Results of proposed method in the presence of Gaussian white noise					(b) Results of proposed method in the presence of Salt & Pepper noise			
Noise variances (σ^2)	SNR	NTD	NFD	NMD	Noise density (d)	NTD	NFD	NMD
0.05	1.4142	11	0	0	0.01	11	0	0
0.1	1.0479	11	0	0	0.05	11	0	0
0.15	0.7940	11	0	0	0.1	11	0	0
0.2	0.6431	11	0	0	0.15	10	0	1
0.25	0.5466	11	2	0	0.2	9	0	2
0.3	0.4806	9	1	2	0.25	7	1	4
0.35	0.4320	9	10	2	0.3	6	3	5

Stage 6: Investigate whether the solution is stationary. If not, consider $n = n + 1$ and repeat the algorithm from the stage 4. (The stationary state is detected when $\|\phi^{n+1} - \phi^n\| < \gamma$, a small threshold, or a maximum number of iterations is reached.)

In the next section, the results of detecting small objects using this new NASTA-based active contour model are presented.

4. Experimental results

In this section, we evaluate the performance of the proposed method for detecting small objects on various synthetic and real images with different clutters, textures and noises. At first, we compare the proposed NASTA model with LIF model for detecting small spots against homogeneously cluttered and textured backgrounds. Next, we examine our model for extracting small objects against a heterogeneously textured background (multiple textures with different clutters). Then, we consider the robustness of the proposed method in the presence of noise. Finally, we test our approach on two sets of real-world images.

4.1. Small object detection against homogeneously cluttered and textured backgrounds

In this experiment, we evaluated the performance of the NASTA model and the LIF model for extracting small targets from cluttered backgrounds. Fig. 3 illustrates the experimental results for the two methods in different images. Also, comparative results of two methods based on the number of true detection (NTD), the number of false detection (NFD) and the number of missed detection (NMD) have been shown in Table 1.

The results of the LIF model are indicated in the Fig. 3(row 3). As shown in this figure, the LIF model cannot truly detect all of the small targets in the cluttered background. With increasing the complexity of the background, the numbers of true detection decrease, and the numbers of false and missed detection rise. Eventually, when the background has severe clutter and noise, the LIF model has absolutely lost the small targets (Fig. 3(row 3(c))). Conversely, proposed method, as shown in Fig. 3(row 4), can correctly find all of the targets in the complex background even though the background is too cluttered (Fig. 3(row 4(c))).

4.2. Small object detection against heterogeneously textured backgrounds

Proposed method can also detect small objects against heterogeneously textured backgrounds. Fig. 4(a) shows an image consisting of some small targets in four textured backgrounds with different clutters. Fig. 4(b) presents surface plot of the intensity values of this image. As it is visible in the Fig. 4(b), the surface plot of intensity values of objects and background are difficultly distinguished from each other. Hence, the LIF model based on intensity values is unable to detect any targets in such cases and targets are completely missed (Fig. 4(d)). However, the proposed method using NASTA values that surface plot of them is indicated in Fig. 4(f), could exactly identify all of the small targets in the heterogeneously textured backgrounds (Fig. 4(e)).

4.3. Considering robustness against noise

To assess the effectiveness of the NASTA method in the presence of noise, we added two types of noise to a grey-level synthetic image (Fig. 5(row 1)) and evaluated the target detection results in the noisy images. In this experiment, the intensity values of the original image vary from 0 to 1 and the pixel values of obtained noisy images are either truncated at 0 or saturated at 1.

At first, we added Gaussian white noise with zero mean and different variances ($\sigma^2 = 0.05, 0.1, \ldots, 0.35$) to the original image (Fig. 5(row 1)) and considered the robustness of the proposed method to the noise. Second row of Fig. 5 indicates three noisy images obtained by adding Gaussian white noise with variances 0.1, 0.2 and 0.3 to the original image. The detection results of the proposed method corresponding to these noisy images have been shown in the third row of Fig. 5. The signal-to-noise ratio (SNR), defined in (Sonka et al., 2007), also the values of NTD, NFD and NMD for noisy images with different variances have been summarized in Table 2(a). As it is visible, whenever the noise power (σ^2) is less than 0.25, all of the targets without any faults have been detected (Fig. 5(row 3 (a), (b))). When the noise power is equal to 0.25, our method could find all of the targets but two false detections have occurred. Once the noise power is equal to 0.3, in spite of being too difficult to detect all the targets with naked eye, proposed method could detect nine of eleven targets (Fig. 5(row 3(c))). For the noise power higher than 0.3, the targets actually invisible for the naked eye and consequently numbers of false detection of proposed method increase.

Then, we added Salt & Pepper noise with different noise density ($d = 0.01, 0.05, 0.1, \ldots, 0.3$) to the original image (Fig. 5(row 1)) and again considered the robustness of the proposed method against the noise. The noisy images and results of detecting targets for $d = 0.05$, 0.15 and 0.25 are illustrated in Fig. 5(row 4) and (row 5) respectively. The values of NTD, NFD and NMD have been determined for the seven values of different noise densities in Table 2(b). As shown, whenever the density of noise is less than 0.15, all of the targets are rightly extracted (Fig. 5(row 5(a))). While, the density of noise is equal to 0.15 and 0.2, one target (Fig. 5(row 5(b))) and two targets are missed respectively. When, the density of noise is equal to 0.25, regardless the severity of finding targets, proposed method could detect seven of eleven targets (Fig. 5(row 5(c))). For the noise density more than 0.25, again the targets are undetectable for the naked eye, and, consequently, NTD is reduced, NFD and NMD are increased.

According to this experiment, the proposed NASTA method has well robust against the additive white Gaussian noise and the Salt & Pepper noise and usually it would be able to find out targets in the images with strong noise.

4.4. Application on real images

In order to show the ability of the proposed method for detecting small objects against cluttered backgrounds on real-world images, we tested our method on a set of real SAR images and also a number of medical images. The SAR images were selected from ADTS[1] dataset collected by the MIT Lincoln Laboratory. We utilized single look

[1] https://www.sdms.afrl.af.mil/index.php?collection=adts.

Table 3
Detection results and computational times of proposed method on real images (Fig. 6).

Image	Number of all targets or spots	NTD	NFD	NMD	Size	Computation time of NASTA image(s)	Number of iterations	Total time(s)
m78p1f23hh	9	8	0	1	400×100	4.81	20	5.64
m78p7f23hh	8	8	0	0	500×125	7.22	11	8.03
m85p3f21hh	7	7	0	0	600×150	10.10	18	12.58
mdb058	4	4	0	0	375×450	18.00	19	23.05
mdb219	1	1	0	0	300×350	11.64	17	14.41
mdb247	2	2	0	0	250×300	8.42	22	11.00

complex (SLC) and HH polarization images in this test. The size of each image in this dataset is 2048×512 pixels, but we resized them ($400 \times 100, 500 \times 125$ or 600×150) for this experiment. The selected images, ground truth images and the target detection results of the NASTA method are shown in Fig. 6(row 1), 6(row 2) and (row 3) respectively. These SAR images contain various small man-made targets (military vehicles and corner reflectors) against cluttered and textured backgrounds. In addition, SAR images are contaminated by speckle noise that can be rather difficult to extract the targets from the background. In spite of these difficulties, our method has truly distinguished the targets from the background (Fig. 6(row 3)).

Moreover, we consider performance of our algorithm on a number of medical mammography images for detecting bright spots that could occasionally be a sign of breast cancer. The mammography images were chosen from MIAS[2] dataset provided by the Mammographic Image Analysis Society. The size of each image in this dataset is 1024×1024 pixels, but we applied selected interest regions and resized version of these images ($375 \times 450, 300 \times 350$ or 250×300) for this test. The mammography images, ground truth images and the spot detection results of the proposed method are displayed in Fig. 6(row 4), (row 5) and (row 6) respectively. As seen in the Fig. 6 (row 4), the spots are very small and usually have low contrast with background, however, our model has correctly extracted them (Fig. 6(row 6)).

Table 3 presents the detection results of proposed method corresponding to the images in Fig. 6. Also, this table shows CPU times for computing NASTA images, number of iterations and total CPU times (including computation times of NASTA images plus evaluation of active contour to reach convergence) for images presented in Fig. 6. The computational times in this experiment were obtained in running the code of proposed algorithm in Matlab 7.10 (R2010a) software on Pentium (R) dual-core machine with 2.2 GHz and 2 GB of memory and the Windows XP operating system. As a result from this table, the computational times for computing NASTA images and total execution times are mainly related to the image size.

5. Conclusion

In this research, we described a novel energy function for a localized region-based active contour model, which can be applied for detecting small objects in a cluttered image. In the proposed scheme, image features are determined by the NASTA values and instead of the image intensities are utilized in the energy function of the active contour model. The NASTA can appropriately reinforce dissimilarities between objects and background and also represses clutter and noise of the image. In this paper, some experiments were presented on synthetic and real images for evaluating performance of the proposed NASTA model and comparing it to the LIF model. The results confirmed accuracy and effectiveness of our method for detecting small objects not only in images with complex and cluttered background but also in images with heterogeneously textured backgrounds. In addition, we considered the performance of our method on noisy images. In this experiment, two types of noise: Gaussian noise and Salt & Pepper noise were tested. Experimental results revealed that the proposed method is more robust against noise and it can correctly identify the desired small objects in the presence of severe noise.

[2] http://peipa.essex.ac.uk/ipa/pix/mias/.

Acknowledgments

The authors would like to thank the anonymous reviewers for valuable comments to improve the quality of the paper.

References

Abouelela, A., Abbas, H.M., Eldeeb, H., Wahdan, A.A., Nassar, S.M., 2005. Automated vision system for localizing structural defects in textile fabrics. Pattern Recognition Lett. 26 (10), 1435–1443.
Aubert, G., Kornprobst, P., 2006. Mathematical Problems in Image Processing: Partial Differential Equations and the Calculus of Variations, Second ed. Springer, New York.
Bottema, M.J., Slavotinek, J.P., 2000. Detection and classification of lobular and DCIS (small cell) microcalcifications in digital mammograms. Pattern Recognition Lett. 21 (13-14), 1209–1214.
Caselles, V., Catté, F., Coll, T., Dibos, F., 1993. A geometric model for active contours in image processing. Numer. Math. 66 (1), 1–31.
Chan, T.F., Vese, L.A., 2001. Active contours without edges. IEEE Trans. Image Process. 10 (2), 266–277.
Darolti, C., Mertins, A., Bodensteiner, C., Hofmann, U.G., 2008. Local region descriptors for active contours evolution. IEEE Trans. Image Process. 17 (12), 2275–2288.
He, L., Zheng, S., Wang, L., 2010. Integrating local distribution information with level set for boundary extraction. J. Vis. Commun. Image Represent. 21 (4), 343–354.
Hua, C., Liqun, G., 2008. Geodesic active contour, inertia and initial speed. Pattern Recognition Lett. 29 (16), 2197–2205.
Huang, S.-q., Liu, D.-z., Gao, G.-q., Guo, X.-j., 2009. A novel method for speckle noise reduction and ship target detection in SAR images. Pattern Recognition 42 (7), 1533–1542.
Kass, M., Witkin, A., Terzopoulos, D., 1988. Snakes: Active contour models. Internat. J. Comput. Vision 1 (4), 321–331.
Lankton, S., Tannenbaum, A., 2008. Localizing region-based active contours. IEEE Trans. Image Process. 17 (11), 2029–2039.
Li, C., Chiu-Yen, K., Gore, J.C., Ding, Z., 2007. Implicit Active Contours Driven by Local Binary Fitting Energy, IEEE Conf. Computer Vision and Pattern Recognition(CVPR '07), Minneapolis, MN, pp. 1–7.
Li, C., Kao, C.-Y., Gore, J.C., Ding, Z., 2008. Minimization of region-scalable fitting energy for image segmentation. IEEE Trans. Image Process. 17 (10), 1940–1949.
Li, C., Xu, C., Gui, C., Fox, M., 2010. Distance regularized level set evolution and its application to image segmentation. IEEE Trans. Image Process. 19 (12), 3243–3254.
Malladi, R., Sethian, J., Vemuri, B., 1995. Shape modeling with front propagation: A level set approach. IEEE Trans. Pattern Anal. Machine Intell. 17 (2), 158–175.
Michailovich, O., Rathi, Y., Tannenbaum, A., 2007. Image segmentation using active contours driven by the Bhattacharyya gradient flow. IEEE Trans. Image Process. 16 (11), 2787–2801.
Mumford, D., Shah, J., 1989. Optimal approximations by piecewise smooth functions and associated variational problems. Comm. Pur. Appl. Math. 42 (5), 577–685.
Ng, H.-F., 2006. Automatic thresholding for defect detection. Pattern Recognition Lett. 27 (14), 1644–1649.
Papoulis, A., Unnikrishna, 2002. Probability Random Variables and Stochastic Processes, Fourth ed. McGraw Hill, New York.
Quellec, G., Russell, S.R., Abramoff, M.D., 2011. Optimal filter framework for automated, instantaneous detection of lesions in retinal images. IEEE Trans. Med. Imaging 30 (2), 523–533.
Rabiner, L., Schafer, R., 1978. Digital Processing of Speech Signals. Prentice Hall, New Jersey.
Savelonas, M.A., Iakovidis, D.K., Maroulis, D., 2008. LBP-guided active contours. Pattern Recognition Lett. 29 (9), 1404–1415.
Shan, H., Ma, J., 2010. Curvelet-based geodesic snakes for image segmentation with multiple objects. Pattern Recognition Lett. 31 (5), 355–360.
Sonka, M., Hlavac, V., Boyle, R., 2007. Image Processing, Analysis, and Machine Vision, 3rd ed. Thomson Learning, Toronto.

Tauber, C., Batatia, H., Ayache, A., 2010. Quasi-automatic initialization for parametric active contours. Pattern Recognition Lett. 31 (1), 83–90.
Tello, M., Lopez-Martinez, C., Mallorqui, J.J., 2005. A novel algorithm for ship detection in SAR imagery based on the wavelet transform. IEEE Geosci. Remote Sens. Lett. 2 (2), 201–205.
Tsai, A., Yezzi, A., Willsky, A., 2001. Curve evolution implementation of the Mumford–Shah functional for image segmentation, denoising, interpolation, and magnification. IEEE Trans. Image Process. 10 (8), 1169–1186.
Vard, A.R., Moallem, P., Nilchi, A.R.N., 2009. Texture-based parametric active contour for target detection and tracking. Internat. J. Imaging Systems Technol. 19 (3), 187–198.
Vese, L., Chan, T., 2002. A multiphase level set framework for image segmentation using the Mumford and Shah model. Internat. J. Comput. Vision 50 (3), 271–293.
Wang, L., He, L., Mishra, A., Li, C., 2009. Active contours driven by local Gaussian distribution fitting energy. Signal Process. 89 (12), 2435–2447.
Wang, X.-F., Huang, D.-S., Xu, H., 2010. An efficient local Chan–Vese model for image segmentation. Pattern Recognition 43 (3), 603–618.
Yezzi, A., Tsai, A., Willsky, A., 2002. A fully global approach to image segmentation via coupled curve evolution equations. J. Vision Comm. Image Represent. 13 (1-2), 195–216.
Zhang, K., Song, H., Zhang, L., 2010a. Active contours driven by local image fitting energy. Pattern Recognition 43 (4), 1199–1206.
Zhang, K., Zhang, L., Song, H., Zhou, W., 2010b. Active contours with selective local or global segmentation: A new formulation and level set method. Image Vision Comput. 28 (4), 668–676.
Zhu, G., Zhang, S., Zeng, Q., Wang, C., 2010. Gradient vector flow active contours with prior directional information. Pattern Recognition Lett. 31 (9), 845–856.